Deep Sea Research (1980)
26A, Suppl.1 (GATE)

INTERNAL WAVE KINEMATICS IN THE UPPER TROPICAL ATLANTIC

R. H. Käse and G. Siedler

Institut für Meereskunde, Düsternbrooker Weg 20, 2300 Kiel, Federal Republic of Germany

ABSTRACT

Horizontal velocity and temperature measurements observed from a two-dimensional array of moored instruments, mooring F1, are analysed to describe the near-surface internal wave field in the GATE (GARP Atlantic Tropical Experiment) C-scale area. Spectral properties indicate strong deviations from the Garrett and Munk (1972, 1975) deep ocean internal wave models. The frequency spectrum in the upper pycnocline is dominated by three energetic bands centered at 0.0127 (inertial frequency), 0.08 (M2-tidal frequency) and 3 cph. The latter frequency band does not correspond to the local Brunt Väisälä frequency (> 10 cph) and contains about one half of the total internal wave energy of fluctuations with periods less than 10 hours. Cross-spectral analysis of the high frequency internal waves yields corresponding wavelengths of order 1 km consistent with westward propagating first mode wave groups, if the effect of Doppler shift due to a strong mean current is taken into account.

INTRODUCTION

The kinematics of internal waves in the deep ocean were modelled by Garrett and Munk (1972) on the basis of measurements from moored and towed instruments of different investigators and from various locations. It appeared that a model frequency-wavenumber spectrum consistent with linear wave theory could be fitted to the then existing internal wave data. Since the model was designed for the deep ocean below the surface layer, density could be assumed to vary slowly with depth, and the WKBJ approximation was used for describing the modal structure. The model was improved with respect to the wavenumber bandwidth and the effect of fine structure by Garrett and Munk (1975), also taking into account dropped measurements. The state of development in the field in 1974, i.e. at the time of GATE, was presented in a special collection of papers (see Briscoe, 1975a).

The above model had resulted in the planning of a major experiment with a moored array, IWEX, designed to obtain a complete 3-dimensional set of current and temperature data series in the deep North Atlantic. This experiment was performed in late 1973 (Briscoe, 1975b), and a model spectrum was fitted to these data, based on linear theory (Müller, Olbers, and Willebrand, 1978). Very few

high quality measurements, however, existed that had been obtained in the near-surface layers over the deep ocean, except for some sets of temperature sensor array data (e.g. Pinkel, 1975; Brekhovskiskh, and others, 1975) and towed thermistor chain data (e.g. Bell, 1976). GATE provided the opportunity to carry out an experiment specifically designed to study the kinematics as well as the generation and dissipation of internal waves in the upper tropical Atlantic.

A two-dimensional array of moored instruments was used to observe the near-surface internal wave field in the GATE C-scale. This paper will first summarize the techniques used and will present background information on the mean density and current field in the experiment area as well as samples of current and temperature time series for the period from 30 August to 18 September 1974. We shall then attempt to identify spectral properties of the near-surface internal wave field that indicate deviations from the usually assumed properties of deep-water internal waves. The question of the generation due to wind stress fluctuations and aspects of the dissipation is discussed by Käse and Olbers (1979) in this volume.

APPROACH

An estimate of the probable scales of high-frequency internal waves with low mode numbers for the GATE C-scale area (Fig. 1) before the experiment led to the requirement of resolving horizontal scales from order (10 m) to order (1 km). Although a 3-dimensional near-surface instrument array would have been the most appropriate design for such measurements, it was not considered feasible with the existing know-how in mooring techniques. It was therefore decided to set a 2-dimensional current/temperature sensor array (mooring F1) spanning the upper 200 m of the water column vertically and 500 m horizontally (Fig. 2). The horizontal line was approximately aligned with the Equatorial Countercurrent. Mooring F1 was launched during GATE Phase III on 30 August 1974 and retrieved on 18 September 1974. Its position was 8°49.9'N, 22°52.6' W.

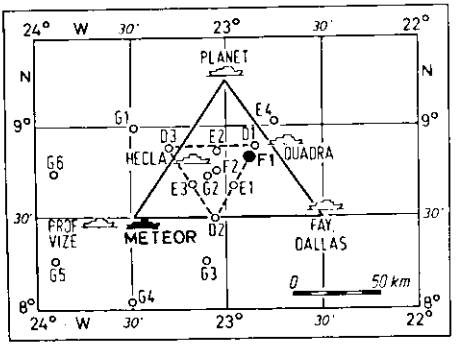

Fig. 1. Positions of two-legged mooring F1 and F.S. Meteor during Phase III in the GATE C-scale area.

Fig. 2. Design of mooring F1: Cable configuration for hypothetical current to the right (a) and instrument and buoy distribution (b).

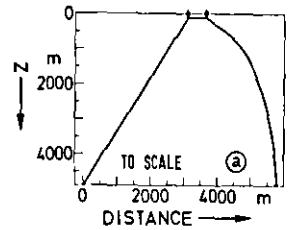

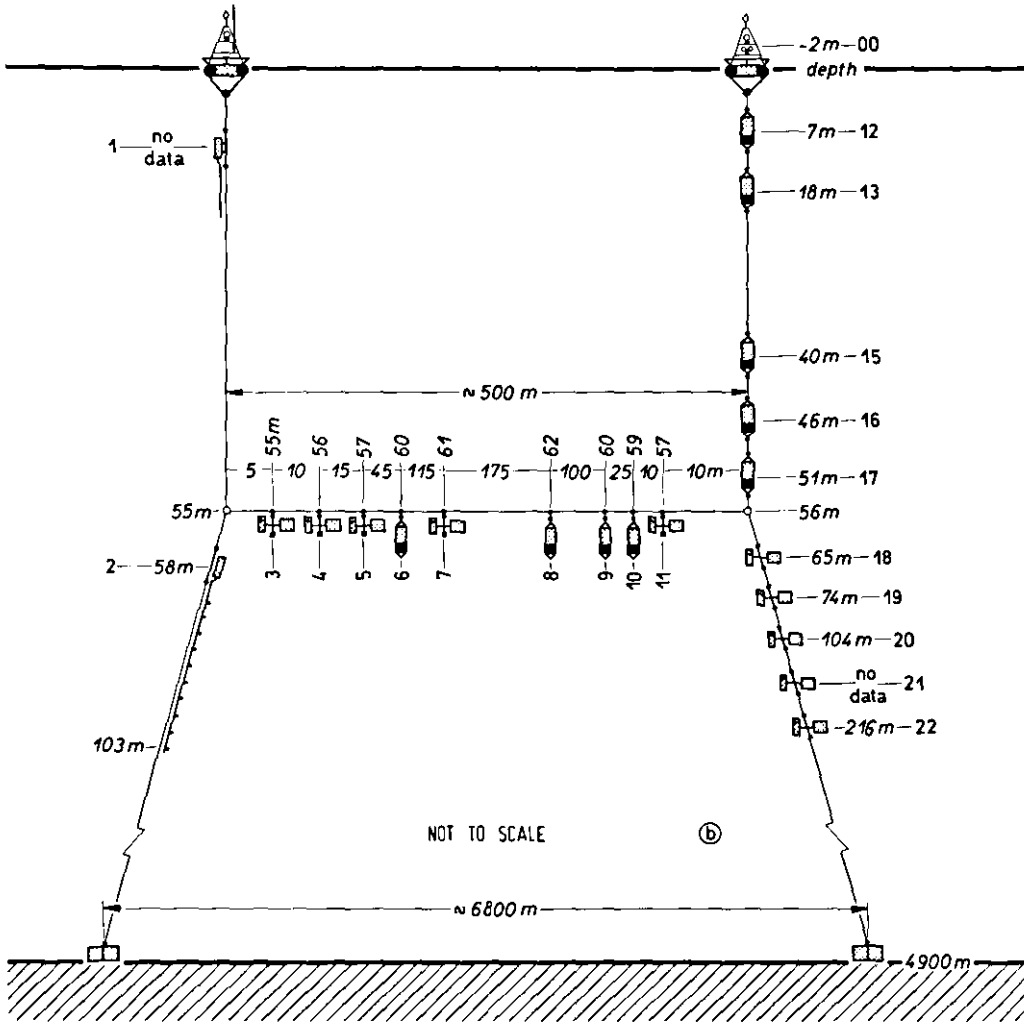

The mooring proved to be an exceptionally stable platform, considering the water depth. Its performance (see. Fig. 3) was described by Siedler and Gerlach (1976), and the data return was summarized by Käse and others (1978). In order to test whether the vertical displacements of moored instruments might seriously contaminate the internal wave results, the spectra of pressure fluctuations indicating vertical instrument motion were compared with water displacement spectra obtained from temperature time series and the mean vertical temperature gradient (Fig. 4). It appears that the mooring noise level is well below the internal wave energy by more than one order of magnitude.

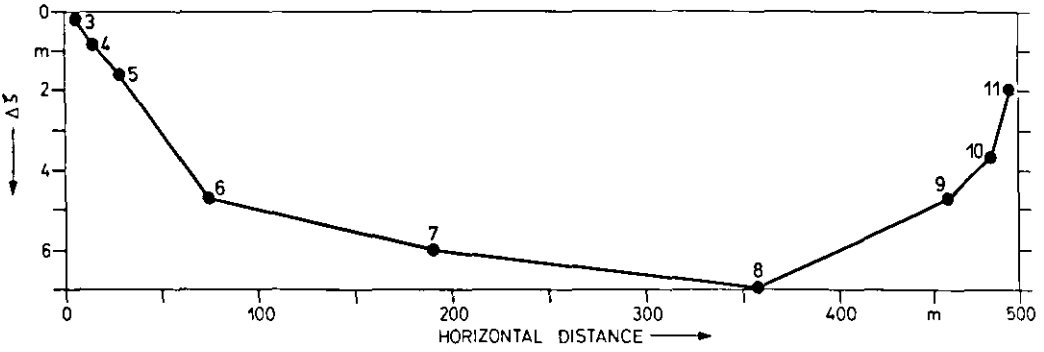

Fig. 3. Depth deviation $\Delta\zeta$ of instruments in horizontal line of mooring F1 estimated from mean temperature profile. Origin corresponds to 56 m.

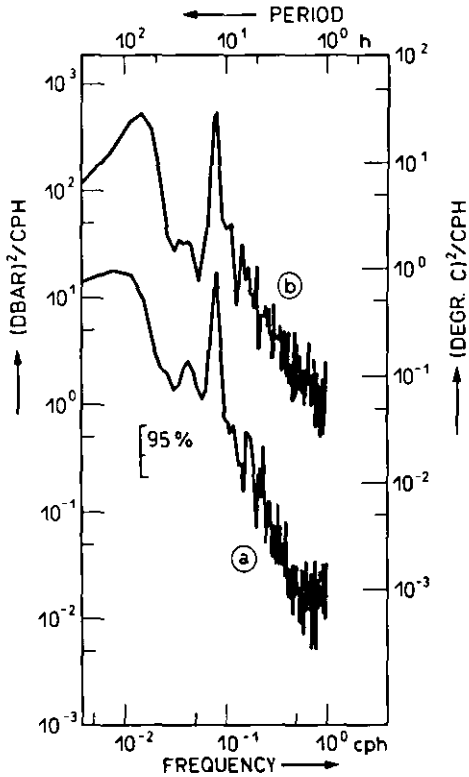

Fig. 4. Frequency spectra of depth fluctuations (a) of instrument 7 in mooring F1 and cf vertical water displacement (b) as calculated from normalised temperature fluctuations.

DENSITY FIELD AND MEAN CURRENTS

The region of observation, approximately situated below the Intertropical Convergence Zone, has some specific hydrographic properties. The surface mixed layer is shallow, typically 30 m, and a strong tropical salinity peak is found just below the mixed layer. Mean vertical profiles of temperature, salinity and density obtained from CTD-measurements on Meteor over 16 days with a sampling rate of 1 hour are shown in Fig. 5. More detailed information on the stratification during the experiment was given by Peters (1978).

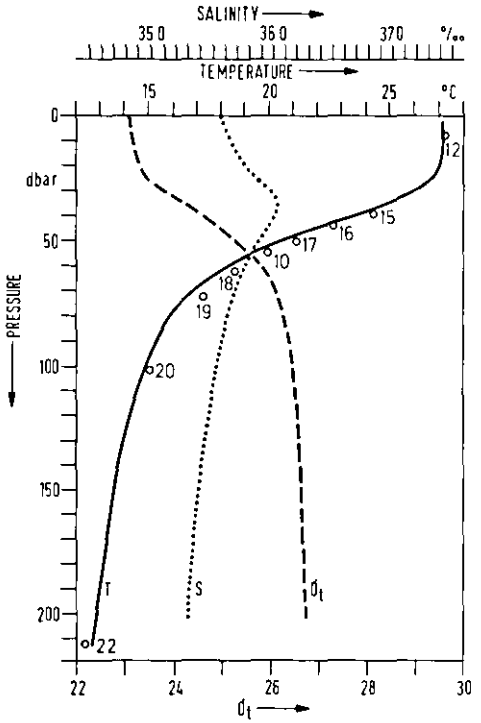

Fig. 5. 16 day average vertical profiles of temperature T, salinity S, and density σ_t obtained from hourly CTD measurements on Meteor. Circles indicate mean values of temperature observed by the instruments of mooring F1.

Since the positions of Meteor and mooring F1 were approximately aligned with the North Equatorial Counter Current, F1 was 75 km downstream of Meteor (see Fig. 1), and it was therefore expected that the temperature stratification would be similar at the two positions. This is indeed the case (see also Clarke, 1979). In Fig. 5 the dots indicate the mean temperatures obtained by averaging F1 data over the whole observation period. It appears that in the maximum gradient layer the temperatures - except for a depth offset of approximately 3 m - agree well with those found by averaging the CTD-profiles

DENSITY FIELD AND MEAN CURRENTS

The region of observation, approximately situated below the Intertropical Convergence Zone, has some specific hydrographic properties. The surface mixed layer is shallow, typically 30 m, and a strong tropical salinity peak is found just below the mixed layer. Mean vertical profiles of temperature, salinity and density obtained from CTD-measurements on Meteor over 16 days with a sampling rate of 1 hour are shown in Fig. 5. More detailed information on the stratification during the experiment was given by Peters (1978).

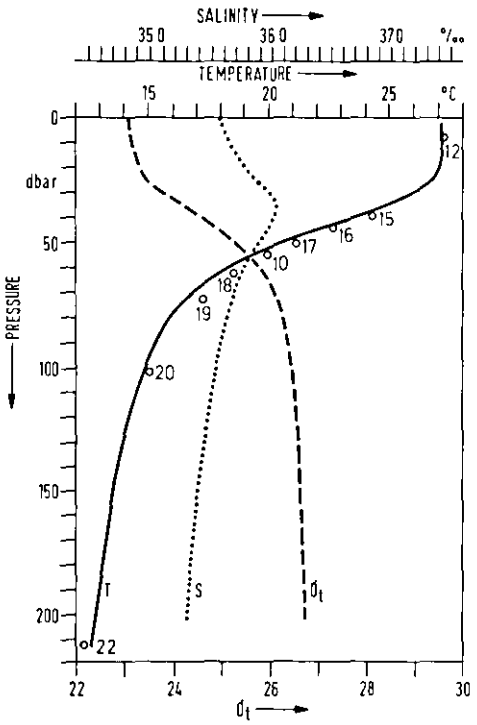

Fig. 5. 16 day average vertical profiles of temperature T, salinity S, and density σ_t obtained from hourly CTD measurements on Meteor. Circles indicate mean values of temperature observed by the instruments of mooring F1.

Since the positions of Meteor and mooring F1 were approximately aligned with the North Equatorial Counter Current, F1 was 75 km downstream of Meteor (see Fig. 1), and it was therefore expected that the temperature stratification would be similar at the two positions. This is indeed the case (see also Clarke, 1979). In Fig. 5 the dots indicate the mean temperatures obtained by averaging F1 data over the whole observation period. It appears that in the maximum gradient layer the temperatures - except for a depth offset of approximately 3 m - agree well with those found by averaging the CTD-profiles

measured on Meteor. The shape of the mean Meteor-profile can therefore be used to calculate the mean vertical temperature gradients at the F1-instrument levels, and the density profile can also be assumed to be correct. The profile of the vertical temperature gradient resulting from averaging Meteor data is presented in Fig. 6a, and a corresponding Brunt-Väisälä frequency profile is shown in Fig. 6b, which was obtained by averaging the depth of selected σ_T-surfaces and consecutive differentiation.

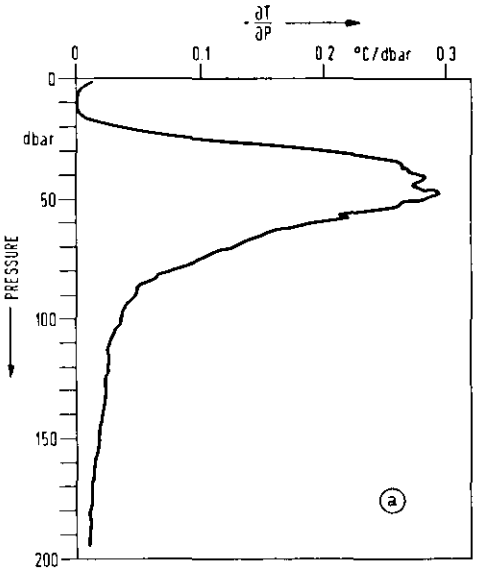

Fig. 6. a) Mean temperature gradient as resulting from Meteor data in Fig. 5.

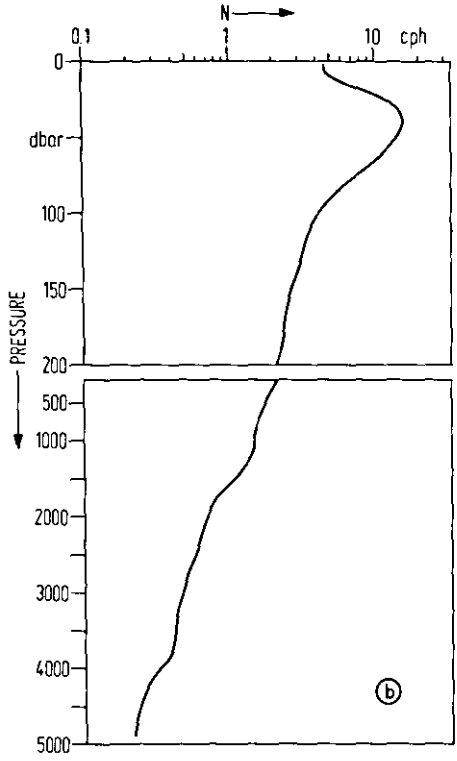

Fig. 6. b) Brunt Väisälä frequency profile calculated with mean Meteor data. Values below 200 m are from one single cast.

The advection of water in the area in GATE Phase III is documented by the progressive vector diagrams in Fig. 7. The mean currents down to 100 m depth are directed towards east-northeast during the observation period, the current at 200 m depth is oriented to the east. Mean speeds are approximately 35-40 cm s^{-1} in the mixed layer and 25 cm s^{-1} at 200 m depth. The variance in the currents is particularly high in the maximum density gradient layer and near the surface. It might be mentioned that the mean current profiles for each observation period varied considerably from GATE Phases I to III (July to September 1974).

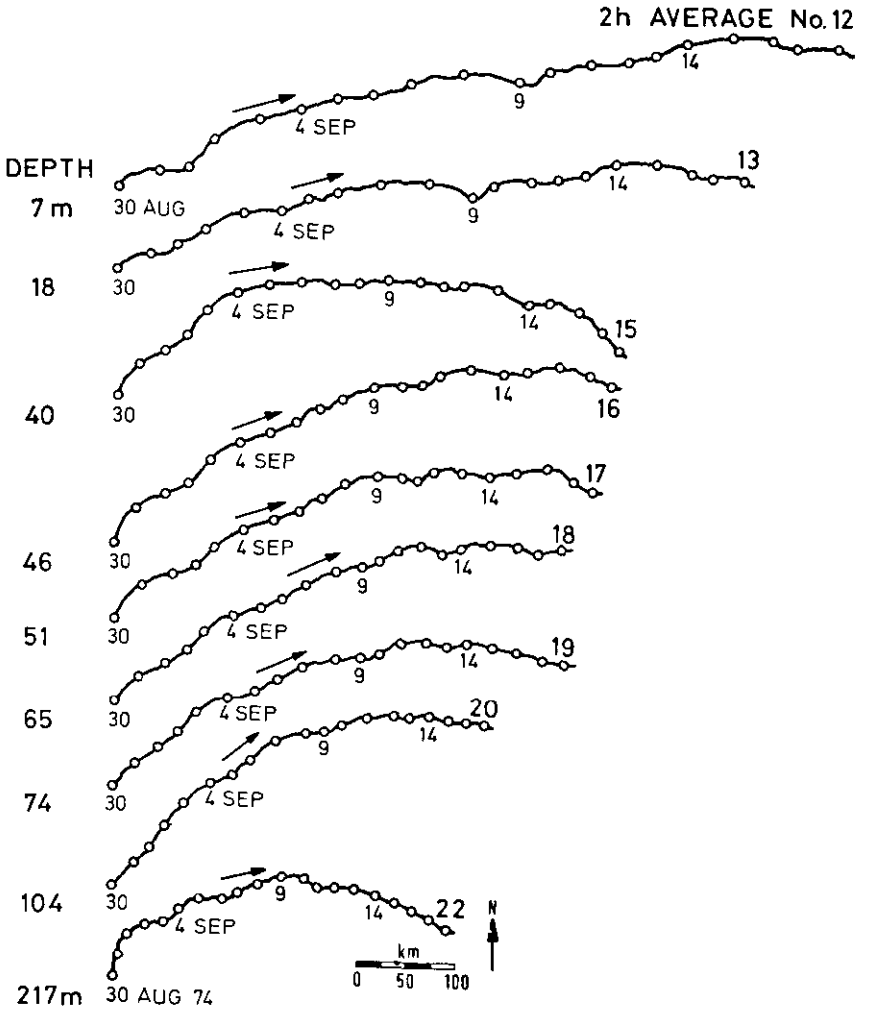

Fig. 7. Progressive vector diagrammes calculated with two-hourly averages of current measurements from instruments in the right leg of mooring F1.

TIME SERIES

Typical properties of the current and temperature fluctuations can be distinguished when inspecting some selected time series from the data set. In Fig. 8 one-hourly averaged time series are presented for the three depth levels 7, 59 and 104 m. Two dominating signals can be found in the plots: a slow variation with a period of 3 days and semi-diurnal signals. As could be expected, the temperature signals are strongest in the high gradient layer. For a selected series from this set, the original non-averaged data were band-pass filtered with the following bandlimits: ∞ - 40 h, 13 - 11 h, and 2 - 1/8 h. The results are plotted in Fig. 9. In addition to the strong signals at inertial (a) and tidal (b) frequencies, considerable fluctuations are found at high frequencies (c).

FREQUENCY SPECTRA

The following analysis is aimed at identifying differences in the spectral properties of deep-water and near-surface internal waves, restricting the discussion to typical features rather than presenting a complete set of energy tests (Müller and Siedler, 1976; Müller, Olbers and Willebrand, 1978).

Since the introduction of the Garrett and Munk (1972) model it became customary to characterize internal wave auto-spectra by simple power laws, usually with a slope of -2 in most of the internal wave band. In addition more or less pronounced maxima are expected at the inertial and tidal frequency (e.g. Briscoe, 1975b). Peaks should then be present at 0.0127 cph (inertial frequency) and at 0.0805 cph (semi-diurnal tidal frequency) in the F1 data set.

Auto-spectra of east- and north current components and of temperature are presented in Fig. 10. These figures were obtained by averaging the spectra of Aanderaa instruments 3, 5, 7, 11 and VACMs 6, 8, 9, 10 (see Fig. 2) and smoothing by a running mean filter, averaging 7 adjacent frequency bands. The most pronounced feature is the strong peak at tidal frequency, which is in agreement with data from other moorings in the GATE C-area (e.g. Perkins and Van Leer, 1977). The peak at inertial frequency is not well resolved due to the strong band averaging. It could, however, already be detected directly in the time series. It should be noted aside that the spectra of both the Aanderaa meters and the VACMs are in remarkably good agreement at frequencies below 0.5 cph, indicating the high stability of the mooring.

A difference to the usual model spectrum is found at high frequencies. The average horizontal kinetic energy spectrum at 56 m depth in Fig. 11 displays a slope less steep than -1.5 in most of the internal wave range, but a significant change in slope at the high frequency end above 1 cph. The decrease in steepness in the log-log-plot corresponds to a major energy peak as can be seen in Fig. 12a where an energy conserving presentation is being used. There are three main peaks in the total energy spectrum: near the inertial frequency, at semi-diurnal tidal frequency and, astonishingly large, near 3 cph. A deviation from a power law at high frequencies was usually attributed to WKBJ turning at the local Brunt-Väisälä frequency N (Desaubies, 1975). The observed local N, however, is larger than 10 cph, and the strong oscillations are probably caused by resonant response of the upper ocean to surface forcing (Käse and Clarke, 1978), with dominant excitation at frequencies near the lower layer N (see Fig. 6b). A similar shape of the spectrum at high frequencies can be found in Pinkel's (1975) data.

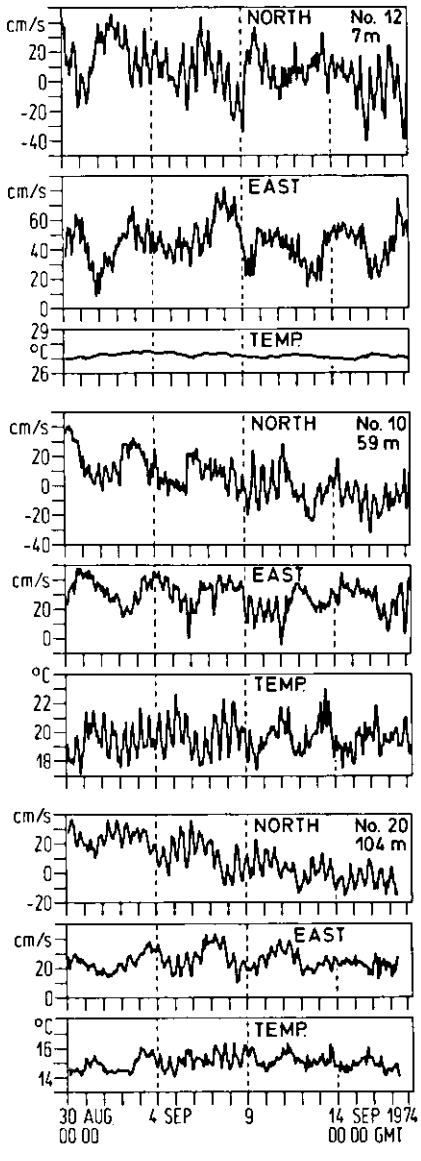

Fig. 8. One-hourly averaged time series of current and temperature signals in the mixed layer, in the maximum gradient layer and below the maximum gradient layer.

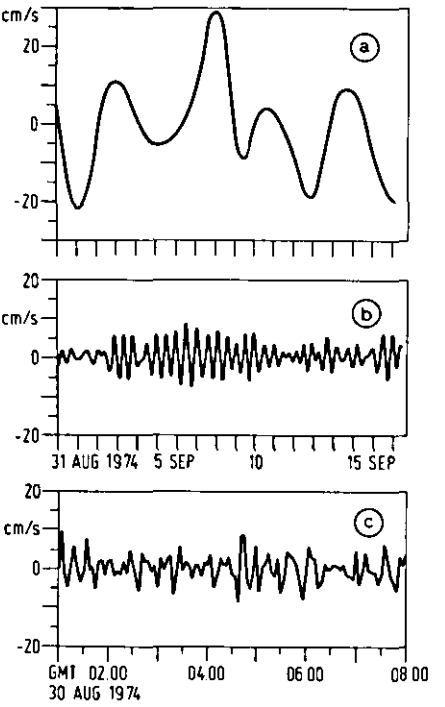

Fig. 9. Band-passed east current component signals of VACM 12 at 7 m depth. Band-limits were a) ∞ - 40 h, b) 13 - 11 h, and c) 2 - 1/8 h. Note different time scale in (c).

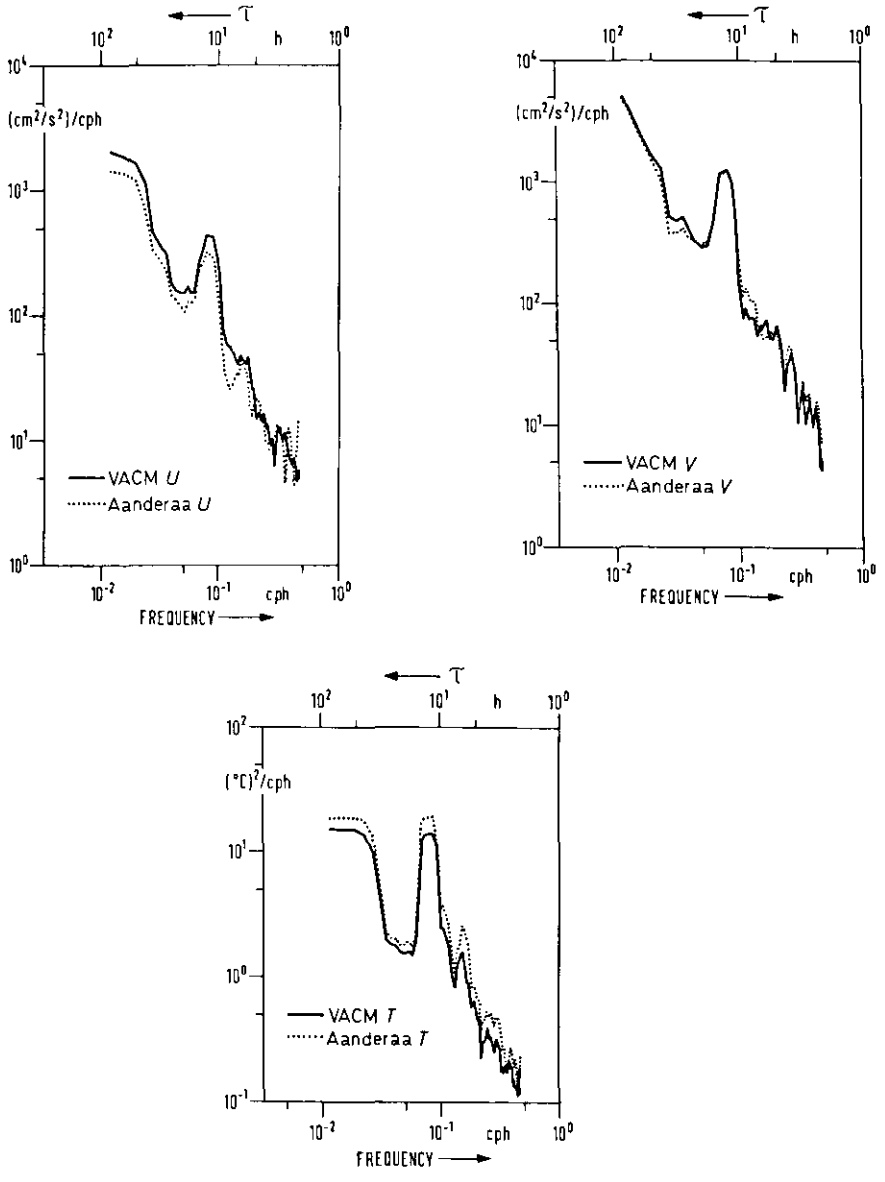

Fig. 10. Auto-spectra of one hourly averaged east and north current components and of temperature at 56 m depth. Full lines represent average spectra of VACMs 6, 8, 9, 10 and dotted lines characterise deviations of the corresponding Aanderaa meters 3, 5, 7, 11. Calculation scheme is described in the text.

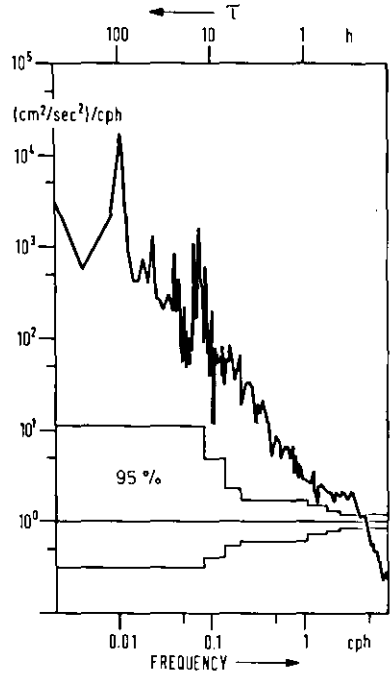

Fig. 11. Horizontal kinetic energy density-spectrum computed for VACM instrument 10.

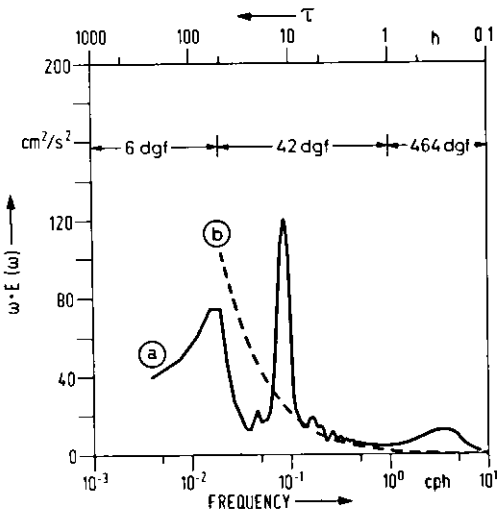

Fig. 12. a) Energy preserving presentation of total internal wave energy E.
Note that $E = 0.5\ (P_{uu} + P_{vv} + (N^2 + \omega^2)\ P_{TT}/\bar{T}_z^{\,2})$ is multiplied by frequency ω and plotted on a linear scale against log ω. Equal area under the curve corresponds to equal energy. A Brunt Väisälä frequency N = 11 cph and a mean temperature gradient $\bar{T}_z$ = 0.25 deg C/m have been used in the computation. The equivalent number of degrees of freedom (dgf) is indicated.
b) Theoretical Garrett-Munk spectrum with energy in the frequency band 0.1 - 1 cph equal to that observed in GATE spectrum (a).

In Fig. 12 b a theoretical Garrett-Munk spectrum with a slope of -2 is given where total energy between 0.1 and 1 cph is equal to the observed GATE spectrum in Fig. 12 a. The relatively large contribution of the total energy at higher frequencies is a consequence of the slow decrease of the GATE spectrum with increasing frequency. Fig. 13 presents an example of the slow variation of energy in the high frequency band with time. There is some indication of a low frequency modulation of this energy peaks at a scale of 3 days which might suggest interaction with inertial currents and/or atmospheric disturbances at that time scale.

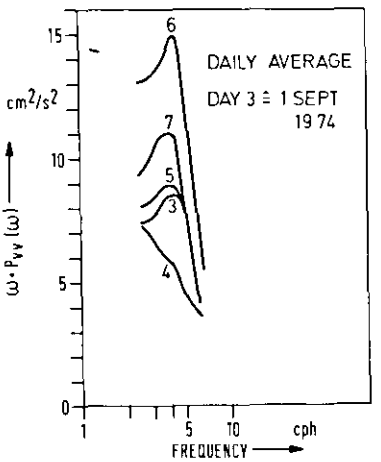

Fig. 13. Variation of high frequency peak in north component current at 59 m. The daily spectra were calculated for 23 overlapped detrended and Hanning windowed pieces of two hours length.

In the near-surface layers one suspects that the usual WKBJ approximation might not be applicable. This is confirmed by a comparison of the energy levels of the currents at 40 and 216 m. They do not differ by more than a factor of 2 (Fig. 14) which should be > 6 if WKBJ theory could be applied, predicting a variation proportional to the local Brunt Väisälä frequency N (Webster, 1969). Obviously a smoothed N profile averaged over a typical low mode number length scale is more appropriate for describing the waves.

The spectra P_{++} and P_{--} of the rotary current components with P_{++} representing anticlockwise and P_{--} clockwise rotating currents (Gonella, 1972) are shown in Fig. 15. If the fluctuations are caused by a random linear internal wave field the ratio P_{++}/P_{--} should vanish at the inertial frequency f and should approach unity for frequencies $\omega >> f$ (Fofonoff, 1969). The ratio resulting from the measured spectra is compared with the theoretical prediction in Fig. 16. Except for frequencies close to f good agreement is found.

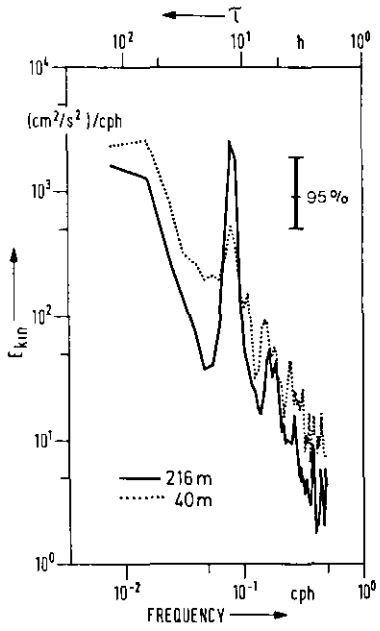

Fig. 14. Horizontal kinetic energy density spectrum at 40 m (VACM 15) and 216 m (Aanderaa 22).

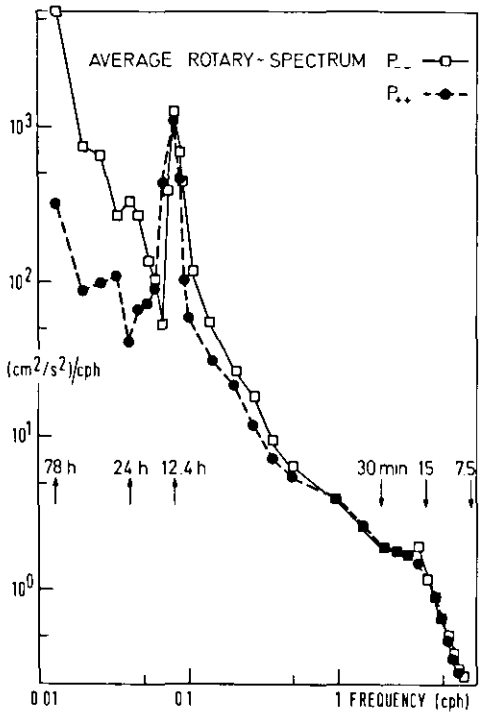

Fig. 15. Anticlockwise (P_{++}) and clockwise (P_{--}) rotary component spectra at 56 m, degrees of freedom as given in Fig. 16.

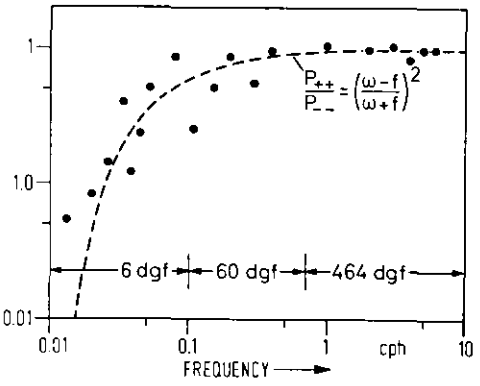

Fig. 16. Ratio P_{++}/P_{--} calculated from observed spectra in Fig. 15 (dots) and theoretical prediction (dashed line) with degrees of freedom (dgf) as indicated. ω and f denote frequency and inertial frequency, respectively.

When comparing the autospectra P_{uu} and P_{vv} of east (u) and north (v) current components one finds no significant difference between these two spectra in the surface mixed layer, but all spectra for depth levels below 40 m exhibit a ratio $P_{vv}/P_{uu} > 1$, indicating anisotropy.

The preceding analysis leads to the conclusion that a large portion of the current and temperature variability in the upper layer is probably caused by inertio-gravitational internal waves. In comparison to results from similar observations in the deeper layers, a high energy range is found at frequencies considerably below the local N and the wave field appears to be anisotropic below the mixed layer. The data set from the moored array also allows one to study the vertical and horizontal spatial structure of the wave field. This will be investigated in the following two chapters.

HORIZONTAL COHERENCE AND PROPAGATION

The results of IWEX already indicated that a better description at high frequencies could be achieved by considering standing normal modes in the vertical rather than propagating waves. Käse and Clarke (1978) suggested a model that describes the 3 cph energy peak in the GATE spectrum in terms of an energetic first mode oscillation.

Atfrequencies below 1 cph the horizontal coherence is always higher than 0.5 (Fig. 17), and major changes in the coherence levels only occur at higher frequencies. Thus, information on the horizontal scales can only be obtained for frequencies above 1 cph for the instrument separations in mooring F1. In Fig. 17 one recognises a tendency to smaller coherence values in current than in the temperature field. This "coherence-disparity" (Briscoe, 1977; Müller, Olbers and Willebrand, 1978) may be attributed to oceanic fine structure, but may also be related to higher mode contributions at depths close to the first-mode zero crossing.

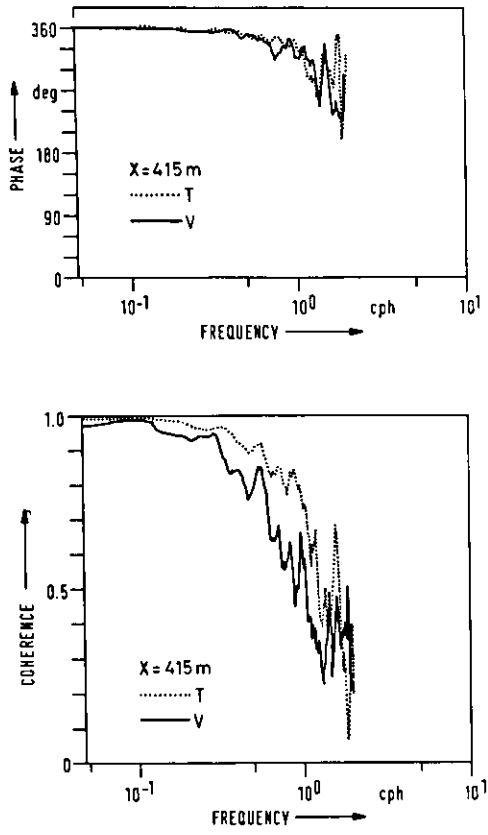

Fig. 17. Coherence and phase of north component current and temperature at a separation of 415 m from VACM instruments 6 and 10. The 95% confidence level for zero coherence is 0.46.

In the case of a dominating first mode some properties of the spatial structure and the propagation characteristics can be deduced from cross-spectral analysis. The cross-spectrum for variables measured at separation X is given by

$$C(\omega,X) - i\,Q\,(\omega,X) = \frac{1}{2\pi}\int_0^{2\pi} E(\omega,\phi)e^{-ik_1(\omega)X\cos\phi}d\phi$$

where C and Q are the co- and quadrature-spectrum, $E\,(\omega,\phi)$ is a directional energy density with the frequency auto-spectrum given by

$$P(\omega) = \frac{1}{2\pi}\int_0^{2\pi} E(\omega,\phi)d\phi,$$

and k_1 is the first-mode scalar wave-number.

For isotropic fields, $Q\,(\omega,X)$ vanishes and $C\,(\omega,X) = J_o(k_1(\omega)\,X)P(\omega)$. The co-spectrum is then an oscillating function of separation X. If the quadrature-spectrum is non-zero and also oscillating, the wave field is directional, and propagation direction and speed can be obtained from the co- and quadrature-spectra. The normalized co-spectrum is shown in Fig. 18. The confidence limit CL was determined from $CL = 1.92/(n-1)^{1/2}$ where n is the number of independent pieces. The negative values of the phase Φ in Fig. 19 indicate prefered propagation to the west. The phase speed may be estimated from the phase Φ by

$$c = \frac{\omega}{\left|\frac{\partial\Phi}{\partial X}\right|}$$

Between 1 and 4 cph a linear regression yields

$$\Phi = -\frac{\omega X}{c}$$

with $c = (1.1 \pm 0.2)$ m s^{-1}. A typical wavenumber $k = \frac{\omega}{c}$ can also be obtained. The first zero crossing of the co-spectrum will occur at X_o where

$$\cos\Phi = 0 \quad \text{or} \quad \frac{\omega X_o}{c} = \frac{\pi}{2}$$

If the wave field is approximated by a single internal wave propagating along the horizontal mooring line (case 1) the estimated wavelength L_o is equal to the wavelength L_1.

However, in the case of propagation from all eastern directions with equal energy partition among different waves (case 2) the cross-spectrum is given by $P(\omega) \cdot (J_o(\hat{k}_1X) + iH_o(\hat{k}_1X))$, where J_o and H_o are Bessel and Struve functions. The phase can be approximated by

$$\Phi \sim -\frac{2}{\pi}\hat{k}_1X.$$

Thus the first zero-crossing will be at $\frac{2}{\pi}\hat{k}_1X_o = \frac{\pi}{2}$ resulting in the corresponding wavelength $\hat{L}_1 \sim 2.5X_o$.

The typical wavelengths L_o obtained at frequencies 2, 2.5 and 3 cph are plotted in Fig. 20 together with the dispersion relationships for the first five normal modes. These were calculated with the N profile of Fig. 6 b assuming vanishing

mean currents. The estimated first mode wavelengths for the two cases lie between the curves for mode one and mode two.

In the foregoing discussion of cross-spectral properties mean currents were neglected. The phase Φ can, however, be influenced considerably by a Doppler shift due to a strong current. Consider a wave field consisting of two waves with equal amplitude and intrinsic wave numbers, propagating in opposite directions. The periodic part is then given by

$$(e^{i\hat{k}_+ X} + e^{i\hat{k}_- X})e^{-i\omega t}, \text{ with intrinsic wavenumbers } \hat{k}_+ = -\hat{k}_-.$$

Although the phase vanishes in the moving frame of reference advected in the positive X-direction by a mean flow U, a non-zero phase will be observed at a fixed point. The apparent wave numbers k_+ and k_- are given by

$$k_+ = \frac{\omega}{c+U} \qquad k_- = -\frac{\omega}{c-U}$$

and the phase is given by

$$1/2\ (k_+ + k_-)\ X = \frac{\omega U}{U^2-c^2} X$$

For $c > U$ the phase is negative, i.e. the apparent wave propagation is upstream, while for $c < U$ the propagation is downstream.

The first mode phase speed is of order O (1 m/s), i.e. larger than the observed mean current of approximately 30 cm/s. Therefore an apparent phase due to the Doppler effect of order

$$O\ (\frac{\omega U}{c^2-U^2} X)$$

is to be expected corresponding to upstream propagation.

The apparent phase due to Doppler shift in case 2 for non-dispersive waves (i.e. constant phase speed c_1) is given by

$$\Phi \sim (\frac{2}{\pi} \frac{\omega X}{c_1} + \frac{U\omega X}{c_1^2})$$

where only linear terms in $\frac{U}{c_1}$ are kept in the calculations.

If the observed wavefield corresponds to the theoretical case 2, the intrinsic wavelength L_1 can be calculated for given mean advection speed U, and the measured phase follows from

$$-\frac{\omega X}{c} = \omega X \cdot (\frac{2}{\pi c_1} + \frac{U}{c_1^2})$$

with $c_1 = \omega L_1/2\pi$. For $c = 1.1$ m/s and $U = 0.3$ m/s one obtains $c_1 = 1.0$ m/s, or wavelengths of 1.8, 1.5 and 1.2 km at frequencies 2, 2.5 and 3 cph corresponding well to the first mode curve in Fig. 20. Thus the Doppler effect can account for the deviations between the observed typical wavelength L_o and the theoretical wavelength for a field without mean current. Considering the magnitude of the effects due to directionality and Doppler shift, values

of L_o given in Fig. 20 are therefore consistent with a dominating first mode. These effects will have an even stronger influence at higher frequencies.

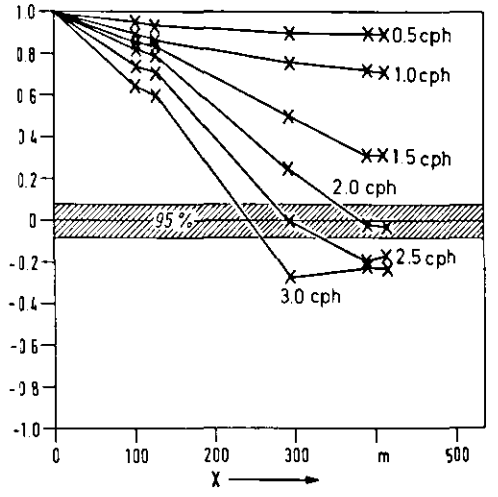

Fig. 18. Normalised temperature co-spectrum as a function of separation for different frequencies.

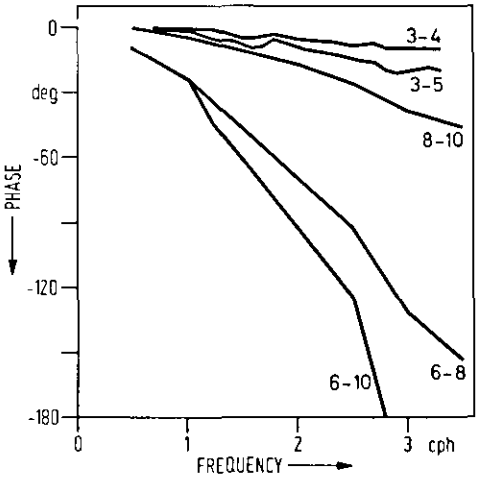

Fig. 19. Phase of temperature cross-spectra for different separations as a function of frequency. The pairs of numbers denote the instruments used. Negative phase means leading of the second instrument.

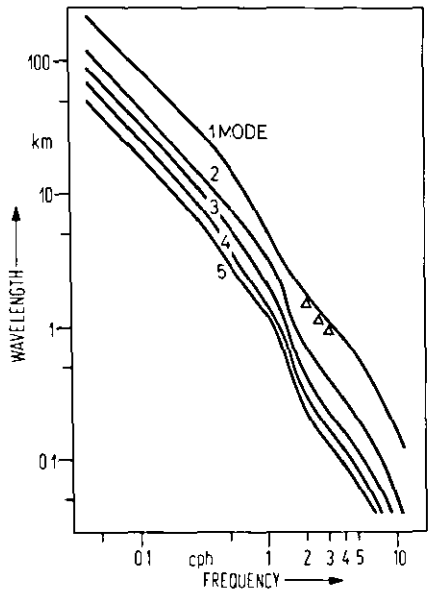

Fig. 20. Theoretical dispersion relationship of first five modes calculated numerically from the mean current-free internal wave equation using Brunt Väisälä frequency of Fig. 6 b. The open triangles result from wavelength estimates (four times the zero crossing distance) of normalised temperature co-spectra in Fig. 18.

VERTICAL COHERENCE

We now check to see if vertical cross-spectral properties are consistent with the findings in the preceding chapter. In the case of a mono-chromatic standing wave the cross-spectrum depends not only on instrument separation but also on the actual depth. Coherences for the same parameters (current, displacement from temperature) should always be one unless one meter is placed at the nodal depth, and phase should be zero or 180 deg, respectively. Although this idealized situation will not exist here and coherence will be below unity, a dominating first mode should determine the phase. However, this cannot be verified from the data because no VACM instruments were moored below 80 m, the nodal depth of a first mode oscillation at 3 cph. As discussed before Aanderaa meter data are too contaminated at frequencies above 0.5 cph to be used for this purpose.

Cross-spectra of current/temperature pairs are usually only analysed for the same instrument, providing information on the isotropy of the wave field. For an anisotropic wave field cross-spectra of current and temperatures for different depth levels must satisfy certain relationships in the case of dominating first mode oscillations. One expects, for example, high coherence of signals at depths of their respective maximum energy. A first mode at 3 cph attains its maximum horizontal velocity in the mixed layer, while temperature has a broad peak in the high gradient layer down to the current's nodal depth. The results of a rotary coherence analysis including the mixed layer instrument 12 and the

instruments 15, 16, and 17 in the maximum N-region are shown in Fig. 21 and indeed yield almost constant current-temperature coherence (Fig. 21a) and decreasing current-current coherence (Fig. 21b). Furthermore, the phases (Fig. 21c) ϕ_+ and ϕ_- of series u + iv and T + iT are required to obey $\phi_+ + \phi_- = 0$. These tests are thus consistent with a dominating anisotropic first mode resulting from the discussion of horizontal coherence.

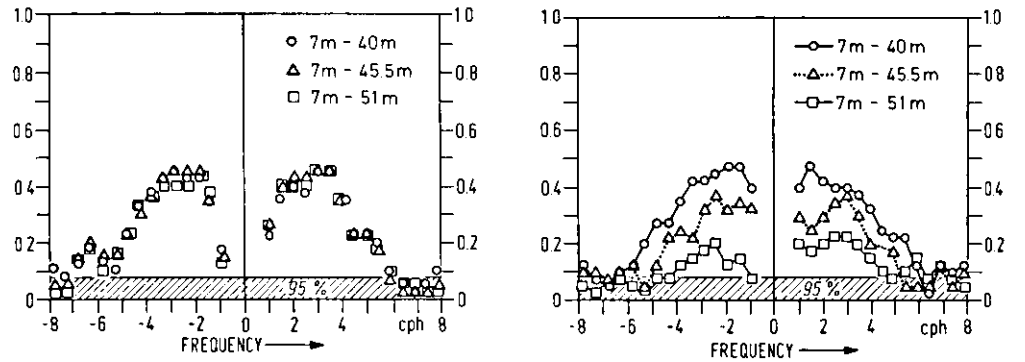

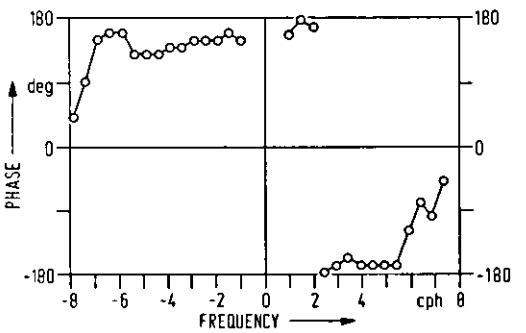

(c)

Fig. 21. Rotary coherence between the mixed layer and 3 levels in the upper thermocline:
a) current-current
b) current-temperature
Phase of cross-spectrum between 7 and 51 m:
c) current-temperature.

DISCUSSION

The observed deviations from the Garrett-Munk spectrum at high frequencies are related to the plateau region of the frequency spectrum around 3 cph. Generally, such discontinuities cause oscillations of the autocorrelation function. These oscillations in the time domain, through the dispersion relationship, have their equivalent in the spatial domain and correspond to propagating wave groups with typical length scales of the inverse wave number bandwidth. This bandwidth can be obtained approximately from the half coherence scale $X_{1/2}$, i.e. the separation where coherence drops below 0.5 (Fig. 22). From the two lines in Fig. 22 it appears that at 1 cph the GATE length scale is as much as 3 times larger than the IWEX length scale. At higher frequencies it decreases faster due to the stronger decrease in the dispersion relationship. A comparison between Figures 20 and 22 leads to the conclusion that the half coherence scale $X_{1/2}$ can approximately be described by

$$X_{1/2} \sim \frac{L_1(\omega)}{2\pi}$$

where L_1 is the first mode wavelength.

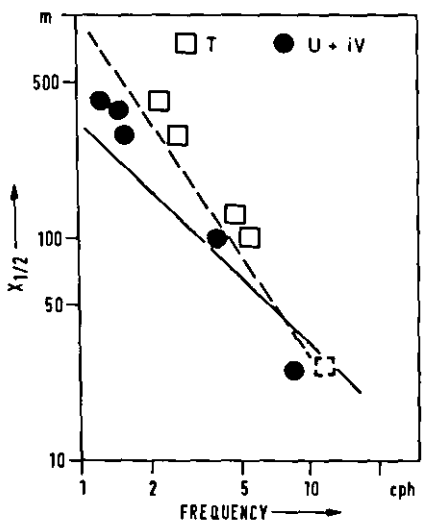

Fig. 22. Half coherence scale $X_{1/2}$ defined as separation at which coherence drops below 0.5 as a function of frequency obtained from current components (U = east, V = north) and temperature T cross-spectral analysis. The dotted box represents an extrapolated value. With units m and cph for $X_{1/2}$ and $\omega/2\pi$, respectively, the solid line results from Briscoe's (1975a) formula

$$(\frac{\omega}{2\pi}) \cdot X_{1/2} \approx 330$$

and the dashed line is given by

$$(\frac{\omega}{2\pi})^{3/2} \cdot X_{1/2} = 1000.$$

The observed change in the slope of the spectrum at high frequency seems to characterize a marked difference in the behaviour of the internal wave field below and above this point. Below this frequency, especially in the inertial range, downward propagating wave groups carry energy from the surface layer to greater depth (Käse and Olbers, 1979). Above 2 cph the waves cannot propagate to deeper regions due to reflection at the turning points and a sudden reduction in vertical internal wave scale can be expected (Siedler, 1971). If the relaxation processes within the upper thermocline have longer time scales than the propagation time of the high frequency waves, multiple reflection and thus resonant forcing of standing modes is possible.

Resonant forcing models such as the linear one by Käse and Clarke (1978) or the weakly non-linear one by Olbers and Herterich (1979) have in common that the energy transfer is most effective for the first mode. It is therefore believed that the preponderance of the fundamental mode is the result of a generation by various sources at those frequencies corresponding to a sudden change in the vertical internal wave scale. In our case it is of the order of the water depth just below 2 cph and is reduced to less than 100 m slightly above 2 cph. The local energy density must increase inversely proportional to this scale if the vertically integrated energy is constant.

The question remains whether the observed directionality is a consequence of preferred generation downstream or whether internal processes cause a directional filtering. In the near-surface region a variety of sources and sinks may exist (Thorpe, 1975), but it is not promising here to search for any single process being responsible for the overall energy transfer. The strong mean current may in many ways interact with the internal wave field (Phillips and others, 1968; Frankignoul, 1974; Müller, 1976). Furthermore, the mean current shear may affect the structure of the internal wave field. It is likely that at times the Richardson Number which on the average over long time periods is much larger than unity (Peters, 1978) drops below critical values when the vertical shear is enhanced by internal waves which were shown to have relatively high energy density on small temporal and spatial scales in the region of this experiment. A study on this aspect of the internal wave kinematics will be the topic of a separate paper.

ACKNOWLEDGMENTS

We appreciated the assistence of the Marine Physics Group at the Institut für Meereskunde Kiel in collecting and processing the data, and we particularly benefited from suggestions by J. Willebrand. This work was supported by the Deutsche Forschungsgemeinschaft Bonn-Bad Godesberg.

REFERENCES

BELL, T.H. (1976). The structure of internal wave spectra as determined from towed thermistor chain measurements. Journal of Geophysical Research, 81, 3709-3714.

BREKHOVSKIKH, L.M., K.V. KONJAEV, K.D. SABININ, and A.A. SERIKOV (1975). Short-Period Internal Waves in the Sea. Journal of Geophysical Research, 80, 856-864.

BRISCOE, M.G. (1975a). Introduction to Collection of Papers on Oceanic Internal Waves. Journal of Geophysical Research, 80, 289-290.

BRISCOE, M.G. (1975b). Preliminary Results From the Trimoored Internal Wave Experiment (IWEX). Journal of Geophysical Research, 80, 3872-3884.

BRISCOE, M.G. (1977). On current finestructure and moored current meter measurements of internal waves. Deep-Sea Research, 24 (12), 1121-1131.

CLARKE, R.A. (1979). Changes in the upper ocean within the C-scale array during phase III. Deep-Sea Research, GATE Supplement I to Vol. 26,115-127.

DESAUBIES, Y.J.F. (1975). A linear theory of internal wave spectra and coherences near the Väisälä frequency. Journal of Geophysical Research, 80 (6), 895-899.

FOFONOFF, N.P. (1969). Spectral characteristics of internal waves in the ocean. Deep-Sea Research, Supplement to Vol. 16, 58-71.

FRANKIGNOUL, C. (1974). Observed Anisotropy of Spectral Characteristics of Internal Waves Induced by Low-Frequency Currents. Journal of Physical Oceanography, 4, 625-634.

GARRETT, C.J.R., and W. MUNK (1972). Space-time scales of internal waves. Geophysical Fluid Dynamics, 2, 225-264.

GARRETT, C.J.R., and W. MUNK (1975). Space-time scales of internal waves: a progress report. Journal of Geophysical Research, 80, 291-298.

GONELLA, J. (1972). A rotary-component method for analysing meteorological and oceanographic vector time series. Deep-Sea Research, 19, 833-846.

KÄSE, R.H., and R.A. CLARKE (1978). High frequency internal waves in the upper thermocline during GATE. Deep-Sea Research, 25, 815-825.

KÄSE, R.H., H. PETERS, G. SIEDLER, and W. ZENK (1978). A compilation of current, temperature and conductivity data from moorings F1 and F2 in the GATE C-area. Meteor Forschungsergebnisse A, 20, 13-48.

KÄSE, R.H., and D.J. OLBERS (1979). Wind-driven inertial waves observed during phase III of GATE. Deep-Sea Research, GATE Supplement I to Vol. 26, 191-216.

MÜLLER, P. (1976). On the diffusion of momentum and mass by internal gravity waves. Journal of Fluid Mechanics, 77, 789-823.

MÜLLER, P., and G. SIEDLER (1976). Consistency relations for internal waves. Deep-Sea Research, 23, 613-628.

MÜLLER, P., D.J. OLBERS, and J. WILLEBRAND (1978). The Iwex Spectrum. Journal of Geophysical Research, 83 (C 1), 479-500.

OLBERS, J.D., and K. HERTERICH (1979). The spectral energy transfer from surface waves to internal waves in the ocean. Journal of Fluid Mechanics, 92, 349-379.

PERKINS, H., and J. VAN LEER (1977). Simultaneous Current-Temperature Profiles in the Equatorial Counter Current. Journal of Physical Oceanography, 7, 264-271.

PETERS, H. (1978). A compilation of CTD- and profiling current meter data from GATE 1974, F.S. "Meteor" and W.F.S. "Planet". Meteor Forschungsergebnisse A, 20, 49-80.

PHILLIPS, O.M., W.K. GEORGE, and R.P. MIED (1968). A note on the interaction between internal gravity waves and currents. Deep-Sea Research, 15, 267-273.

PINKEL, R. (1975). Upper ocean internal wave observation from FLIP. Journal of Geophysical Research, 80, 3829-3910.

SIEDLER, G. (1971). Vertical coherence of short-periodic current variations. Deep-Sea Research, 18, 179-191.

SIEDLER, G., and E. GERLACH (1976). Verankerte Meßsysteme für die Tiefsee - Deep Sea Moorings. Transactions Interocean '76, Düsseldorf, 925-940.

THORPE, S.A. (1975). The excitation, dissipation, and interaction of internal waves in the deep ocean. Journal of Geophysical Research, 80, 328-338.

WEBSTER, F. (1969). Vertical profiles of horizontal ocean currents. Deep-Sea Research, 16, 85-98.

Received 10 April 1979, accepted in revised form 17 September 1979.